Intracellular Accumulation-Driven Potentiation of Moxifloxacin Against non-replicating drug-tolerant *Mycobacterium tuberculosis* through a Prodrug

T. Anand Kumar,[a] Piyali Mukherjee,[b] M. SharathChandra,[c] Shalini Birua,[b] Grace Kaul,[d,e] Abdul Akhir,[d] Sidharth Chopra,[d,e] Jennifer Hirschi,[c]* Amit Singh,[b]* and Harinath Chakrapani[a]*

[a]Department of Chemistry, Indian Institute of Science Education and Research (IISER), Pune, India; [d]Division of Microbiology and Cell Biology, Indian Institute of Science, Bangalore, India; [c]Department of Chemistry, Binghamton University, New York, USA; [d]Division of Molecular Microbiology and Immunology, CSIR-Central Drug Research Institute, Janakipuram Extension, Sitapur Road, Lucknow-226031, Uttar Pradesh, India; [e]Academy of Scientific and Innovative Research (AcSIR), Ghaziabad 201002, India

KEYWORDS. Latent tuberculosis, persisters, mycobacteria, fluoroquinolone, permeability, drug accumulation, phenotypic antimicrobial resistance

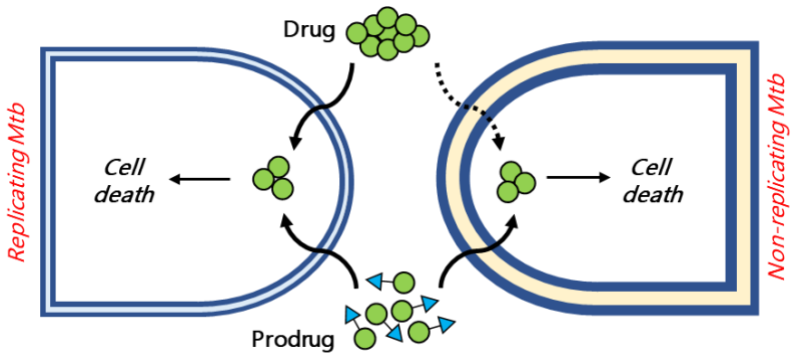

ABSTRACT

During tuberculosis (TB) infection caused by *Mycobacterium tuberculosis* (*Mtb*), a sub-population of mycobacteria can enter a non-replicating persistent state that is not susceptible to most frontline TB drugs, resulting in phenotypic antimicrobial resistance (AMR), which contributes to an extended duration of TB therapy, frequent non-compliance and disease relapse. Recent clinical trial data indicated that inclusion of the fluoroquinolone Moxifloxacin (MXF) led to a shortening of TB treatment from 6-months to 4-months. MXF, however, has limited efficacy on *Mtb* persisting in a hypoxic environment. Here, we report a prodrug approach significantly enhancing MXF's lethality against non-replicating hypoxic *Mtb* while retaining its effectiveness against replicating *Mtb*. Since hypoxia is associated with a reductive environment and induces the expression of reductive enzymes such as nitroreducatases (NTRs) in *Mtb*, we designed and synthesized a library of nitroaryl and nitroheteroaryl conjugates of MXF. After optimization of several factors, including reduction potential, rate, and efficiency of drug release, as well as selectivity, we identified 2-nitrothiazole-derivative as a prodrug that is rapidly and nearly quantitatively converted to MXF in the presence of NTR. Biochemical studies supported by computational data reveal a rate-limiting influence of electron transfer in the mechanistic pathway for activation of the nitroaryl group, a key step in prodrug activation leading to drug release. The lead prodrug's potency against replicating bacteria in both cellular and animal model studies, and mode of action is nearly identical to MXF with significantly higher lethality against non-replicating *Mtb* than MXF. The prodrug showed improved accumulation of MXF inside non-replicating *Mtb* when compared with MXF alone, likely due to the prodrug's ability to enhance accumulation of MXF within non-replicating *Mtb*. Hence, together, the newly developed 2-nitrothiazole-prodrug is rapidly, efficiently, and selectively cleaved under reductive conditions to produce the active drug and had superior permeability and accumulation in non-replicating *Mtb*, which likely contributes to its increased efficacy.

This proof-of-concept study supports prodrug approaches with a focus on improving accumulation of the active drug within non-replicating pathogens as a strategy to address phenotypic AMR.

INTRODUCTION

Tuberculosis, a deadly infectious disease caused by *Mycobacterium tuberculosis* (*Mtb*), is among the leading causes of death globally.[1,2] Although curable through a chemotherapeutic regimen of 6 months, efforts are on to reduce the treatment time, compliance, and relapse while addressing the growing incidences of drug resistance.[1,3] One important feature about *Mtb* is that a fraction of mycobacteria goes into a non-replicating state wherein bacterial cells are tolerant to clinically-relevant anti-TB drugs.[4] These cells are genetically identical to the rest of the population but are phenotypically slow growing and enter a metabolically quiescent state in response to immune pressures (e.g., IFN-γ).[5,6] This phenotypic form of antimicrobial resistance (AMR) is associated with a reduced metabolic rate, activated stress response, altered cell-wall permeability, and heightened drug-efflux activity as compared to drug-susceptible mycobacteria and contribute to the protracted anti-TB regimen and play a significant role in relapse (Figure 1a).[7–12] Hence, strategies that can eliminate phenotypic AMR are in urgent need.

In a recent clinical trial, reduction of therapy duration form 6 months to 4 months was achieved by the use of Rifapentine and Moxifloxacin (MXF).[13] However, MXF's lethality against non-replicating *Mtb* is diminished when compared with replicating *Mtb*.[14,15] Since MXF's target, DNA gyrase, which controls bacterial DNA topology by breaking DNA, passing duplex DNA through the break, and then resealing the gap, is expressed in the non-replicating phase, reduced drug-target engagement contributes to diminished potency in non-replicating *Mtb*.[16–18] One characteristic feature of non-replicating *Mtb* is the increase in thickening of cell wall and

negative zeta potential as a result of an accumulation of polysaccharide and lipid content.[12,19] Reduced intracellular accumulation has been reported for several drugs, including MXF, and this contributes to decreased potency against non-replicating *Mtb*[14]. MXF is relatively hydrophilic (clogP, -0.49) and also exists in pH 7.4 as a carboxylate (p*K*a of the acid is 6.25)[20] and these together likely diminish intracellular accumulation. We considered a prodrug approach to enhance MXF's efficacy by improving permeability and intracellular drug accumulation in non-replicating *Mtb*.

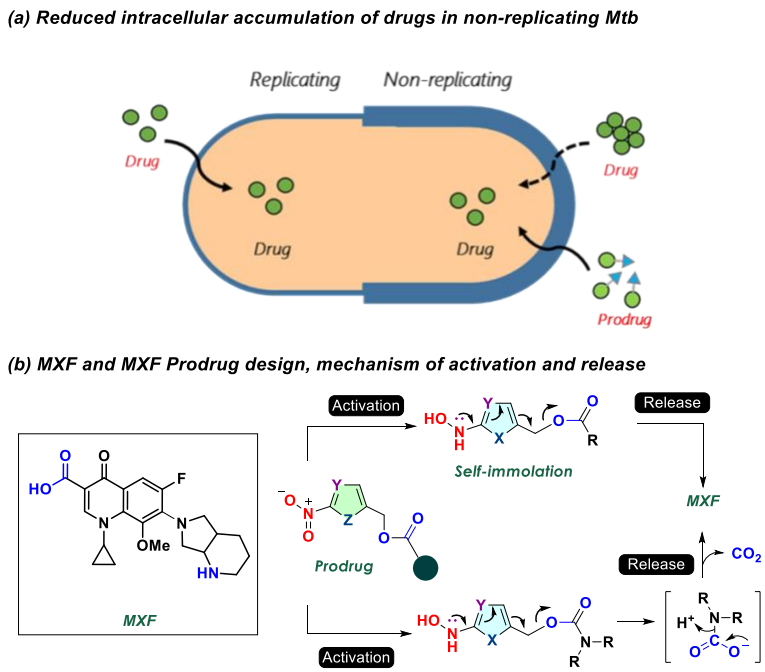

Figure 1. (a) Proposed prodrug strategy to enhance the accumulation of a drug in non-replicating *Mtb*. Non-replicating *Mtb* display a distinctive phenotypic heterogeneity through enhanced cell wall thickness, which may reduce drug uptake. (b) Structures of MXF and its prodrugs (ester and carbamate). (c) Proposed strategy for the generation of MXF following bioreductive activation of nitroheteroaryl ester and carbamate prodrugs. Reduction of prodrug results in the formation of hydroxylamine intermediate, which upon subsequent self-immolation releases MXF.

Within caseating/necrotic TB lesions, non-replicating *Mtb* persists in areas of low oxygen tension, and as a consequence, grows in a bioreductive environment.[21,22] Comparative gene-expression analysis between replicating and non-replicating *Mtb* reveals the over-expression

of reductive enzymes such as nitroreductases.[23,24] These enzymes become good pharmacological targets in bacteria-specific drug delivery and imaging. We therefore considered a MXF prodrug that can be cleaved by nitroreductases to generate the active drug for counteracting phenotypic AMR in *Mtb*. A suitably connected nitro(hetero)aryl group allows for the release of MXF, only after reduction of the nitro group to an electron rich hydroxylamino or amino group (Figure 1b). Since bacterial nitroreductases are also prevalent in replicating bacteria, such compounds are expected to generate MXF in actively replicating bacteria as well and hence, the prodrugs should retain their potency. Here, we designed and developed a prodrug of MXF that undergoes rapid and efficient cleavage under bioreductive conditions to produce MXF, provide chemical and biochemical insights into the prodrug activation and release mechanism, and identify a lead compound that had superior efficacy against non-replicating *Mtb* while retaining activity against actively replicating *Mtb*.

RESULTS

Synthesis, physicochemical properties and reduction potential. The *t*-Boc protected MXF derivative **4** was prepared using a reported procedure.[25] Esterification of this compound using the corresponding nitroaryl or nitroheteroaryl alcohol afforded analogues **3a-3e (Scheme 1)**. Deprotection of the *t*-Boc group gave the desired compounds **1a-1e (Scheme 1)**. As an alternative strategy, we considered carbamates as potential prodrugs (Figure 1b). Fragmentation of the carbamate linkage initiated by the nitro group reduction results in the formation of MXF with the loss of CO_2. As a model substrate, the 4-nitrophenyl based carbamate derivative, **2a** was synthesized from MXF (Scheme 1)**.**

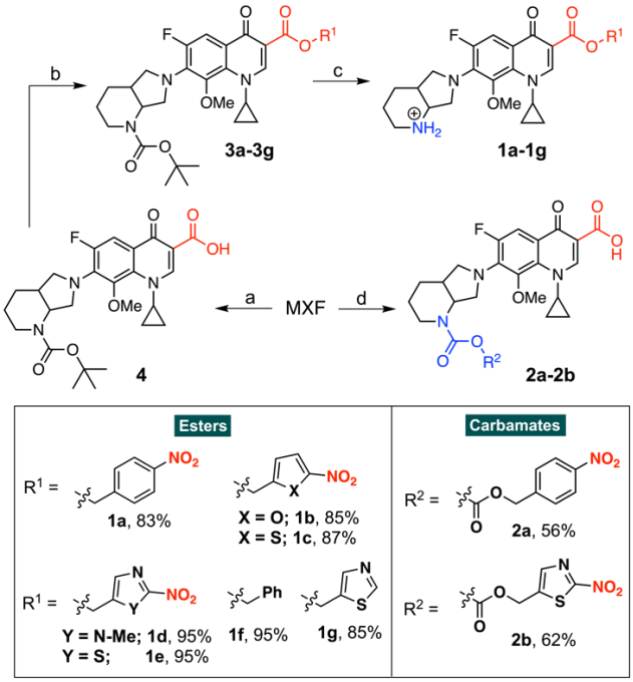

Scheme 1. General procedure for the Synthesis of prodrugs: (a) $(Boc)_2O$, NaOH, H_2O:dioxane (1:1 v/v); (b) R^1OH, HBTU, DMAP, DIPEA, DCM; (c) TFA, DCM; (d) *p*NO_2PhOR^2, Et_3N, DMF.

The clogP for derivatives **1a-1e**, and **2a** was determined by ChemDraw 19.1 and as expected, these derivatives had a higher clogP than MXF (Table 1). Next, guided by a recent and comprehensive study on the effect of physicochemical properties on drug accumulation determined that, in addition to clogP, molar refractivity (MR) and topological polar surface area (TPSA) were important predictors of drug accumulation in bacteria.[26] Using SwissADME,[27] we calculated the molar refractivity (MR) and topological polar surface area (TPSA). For compounds **1a-1e** and **2a**, both MR and TPSA were significantly higher (Table 1) when compared with MXF suggesting improved permeability and accumulation of these compounds.

The reduction of the nitro aryl group triggers the release of MXF, which is expected to depend on the reduction potential of the nitroaryl functional group. Cyclic voltametric analysis revealed that the nitroaryl derivative showed a well-defined cathodic peak, that is consistent

with an irreversible nitro group reduction (Figure S1). The reduction potentials ($E°_{red,}$ Exptl) for compounds **1a**-**1e** and **2a** were found to be -1.21 V to -0.63 V (Table 1).

Table 1. Physicochemical properties and reduction potentials of compounds prepared in this study

Cpd	clogP[a]	MR[b]	TPSA[c]	$E°_{red}$ (V)	
				Exptl[d]	Theory[e]
1a	3.0	164.3	163.3	-0.96	-0.88
1b	2.0	156.6	176.4	-0.81	-0.92
1c	2.5	162.2	191.5	-0.88	-0.96
1d	0.7	161.4	181.1	-0.95	-1.01
1e	1.0	160.0	204.4	-0.63	-0.55
2a	4.4	158.7	147.1	-1.21	-1.24
2b	2.6	154.4	188.2	-0.83	-1.03
MXF	-0.49	120.8	88.3	-	-

[a]clogP values were obtained using ChemDraw 19.1 for prodrugs/drug; [b]MR = molar refractivity (represents the molar volume of the molecule); [c]TPSA = topological polar surface area (represents the surface sum over all polar atoms or molecules); [d]experimentally determined onset reduction potentials using cyclic voltammetry and [e]computed reduction potentials are reported in volts (V).

We also computed the reduction potentials of our target molecules using wB97XD/aug-cc-pVDZ//B3LYP/6-31G(d)[28–30] (Table 1), which were in excellent agreement with the $E°_{red,}$ Exptl for compounds **1a**-**1e** and **2a** (Figure S2). The 2-nitrothiazole derivative, **1e** has the lowest reduction potential of -0.63 V (-0.55 V theoretical) indicating that the reduction of this compound is thermodynamically the most feasible in the series (Table 1 and Figure S1-S2). Based on this observation, compound **2b**, with the 2-nitrothioazole functional group was synthesized (Scheme 1). This compound had similarly favorable physicochemical properties and was also among the compounds with a lower reduction potential (-0.83 V, exptl; -1.03 V,

theory). Overall, our analysis predicts the 2-nitrothiazolyl group to undergo facile reduction. As a control, two compounds **1f** and **1g** without the nitro group were prepared and hence are not expected to get activated through bioreduction to produce MXF (Scheme 1).

MXF release from prodrugs under chemoreductive and bioreductive conditions. We next assessed the ability of these derivatives to undergo cleavage under chemoreductive and bioreductive conditions to produce MXF. Previous reports show that MXF in pH 7.4 buffer is fluorescent (λ_{ex} = 289 nm and λ_{em} = 488 nm, ϕ_F = 0.21, Figure S3).[31] We found that the MXF derivatives **1** and **2** were themselves only mildly fluorescent and hence enhancement in fluorescence in the presence of the reducing agent would be a good estimate for MXF yield. First, with sodium dithionite ($Na_2S_2O_4$),[32] which mimics bioreductive conditions prevalent in hypoxic areas, an enhancement in fluorescence attributable to MXF formation was observed supporting that all nitroaryl compounds generated MXF (Table 2 and Figure S4A). Similarly, with zinc (Zn) and ammonium formate ($HCOONH_4$; AF),[33] which has also been used to simulate bioreductive conditions, the formation of MXF was observed (Table 2 and Figure S4B). The yields of MXF in both experiments were in the range 24-78%, as determined by fluorescence standard curve with authentic MXF. The time course of MXF release following dithionite induced reduction showed that **1e** rapidly (< 5 min, Figure S5A) and in a dose-dependent manner (Figure S5B) underwent reduction to produce MXF when compared to other compounds tested. Under Zn/AF conditions, a similar profile for **1e** was recorded (Figure S5C). In order to assess the correlation between chemoreduction and enzymatic bioreduction, the formation of MXF in the presence of commercially available *E. coli* nitroreductase (NTR) was recorded. Under these conditions, yields ranging from 3-86% were noted with **1e** and **2b** being the most efficient generators of MXF (Table 2 and Figure S6A). Lastly, in order to estimate MXF yields under mycobacterial enzymatic reductive environment, we used whole cell lysate of *Mycobacterium smegmatis* (*Msm*) (Table 2 and Figure S6B): MXF yields ranged from 6-

61%. Together, these data demonstrate a high degree of variability in the yields of MXF under chemo- and bio-reductive conditions and hence a comprehensive evaluation is necessary. For instance, 1-methyl-2-nitroimidazole functional group has been previously shown to be the most efficient substrate for reductive activation of prodrugs.[34-36] However, our data shows that 1-methyl-2-nitroimidazole prodrug **1d** gave higher yields of MXF under chemoreductive conditions but diminished yields under bioreductive conditions (Table 2). On the other hand, the yields of MXF from 2-nitrothiazole prodrug **1e** and **2b** was uniformly higher (Table 2), suggesting the superiority of the newly developed 2-nitrothiazole caging group for use in bacteria. A recent study shows the utility of 2-nitrothiazole for prodrug activation under hypoxic conditions.[37] As expected, the negative control compounds **1f** and **1g** did not produce MXF under any of the aforementioned reductive conditions highlighting the importance of the nitroaryl group in activation and MXF release (Figures S4 and S6).

Table 2. Yields of MXF under reductive conditions monitored by MXF fluorescence enhancement

Cpd	Chemoreduction		Bioreduction	
	$Na_2S_2O_4$[a]	Zn[b]	NTR[c]	*Msm*[d]
1a	55	68	13	6
1b	48	53	8	27
1c	57	56	64	25
1d	32	78	7	18
1e	53	78	86	61
2a	24	29	3	9
2b	39	71	49	53

[a-b]Reductive activation of prodrugs was evaluated by fluorescent measurement of MXF (λ_{ex} = 289 nm and λ_{em} = 488 nm) generated during incubation of **1a-1e** and **2a-2b** (10 μM) under chemoreductive conditions ([a]sodium dithionite and [b]Zn/AF) and [c-d]bioreductive conditions ([c]with *E. coli* NTR (15 nM) and NADH (100 μM) in pH 7.4 phosphate buffer; and [d]with whole cell lysates of *Mycobacterium smegmatis* (*Msm*) for 1 h.

To gain a better understanding of the differences in the rate of NTR catalyzed nitroreduction of prodrugs, the kinetics of MXF release was studied. While previous studies with similar nitroaryl compounds used a concentration of 41.6-100 nM NTR,[34-36] we chose a lower concentration of NTR of 15 nM that provides a more accurate estimate of sensitivity of the substrate towards catalysis by NTR. Initial reaction rates were obtained from the linear portion of the experimental progress curves and these data were fitted into the Michaelis-Menten equation. A significant difference in rates among these compounds was recorded, with **1e** and **2b** being the best substrates for NTR (Figure 2 and Table 3).

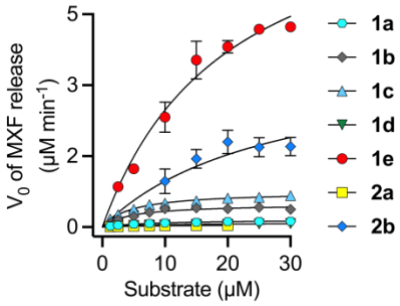

Figure 2. Michaelis-Menten plots of enzyme kinetics using prodrugs **1a-1e**, **2a** and **2b** with *E. coli* NTR. Values are averages (n = 3, mean ± SD)

Table 3. Kinetic parameters for NTR-catalyzed reactions

Entry	Cpd	k_{cat}[a]	K_m[b]	k_{cat}/K_m[c]	Driving force[d]
1	**1a**	10	7.28	1.4	-1.8
2	**1b**	37	5.98	6	-5.3
3	**1c**	52	5.08	10	-3.7
4	**1d**	6	9.59	0.6	-2.1
5	**1e**	494	19.81	25	-9.5
6	**2a**	3	6.66	4	3.9
7	**2b**	219	22.5	9.7	-4.8

[a]min^{-1}; [b]μM (data with estimates of error are available in the SI, Table S1); [c]μM^{-1} min^{-1}; [d]kcal/mol.

Lineweaver-Burk plots gave k_{cat} and K_m (Figure S7 for individual data plots; Table 3), and analysis of kinetic parameter k_{cat}/K_m showed the superiority of 2-nitrothiazole prodrugs over other compounds tested (Figure S7, S8 and Table 3, entries 5 and 7). Contrary to previous work and in line with data from our bioreductive experiments, we found that 2-nitroimidazole MXF prodrug **1d** had diminished efficiency of reduction and lower yields of the payload when compared with other prodrugs tested.[34–36] Lastly, molecular dynamics simulations with NTR and FMN cofactor along with the docked substrates in the active site were carried out and the driving force for electron transfer from FMN to the nitro group was determined (Table 3). A moderate correlation (R^2 value of 0.75; Figure S9) between the computed driving force and catalytic efficiency (k_{cat}/K_m) supports the importance of electron transfer in prodrug activation.

Bioreductive activation of 1e. Based on a threshold of 50% yield in all reductive assays and rates of above 0.5 μM min^{-1}, the prodrug **1e** was identified as the lead molecule for further evaluation. Fluorescence analysis with NTR showed rapid activation and nearly complete conversion to MXF in less than 30 s (Figure 3A and Figure S10). LC/MS analysis of a reaction mixture showed nearly quantitative conversion of **1e** to MXF (Figure 3B and S11).

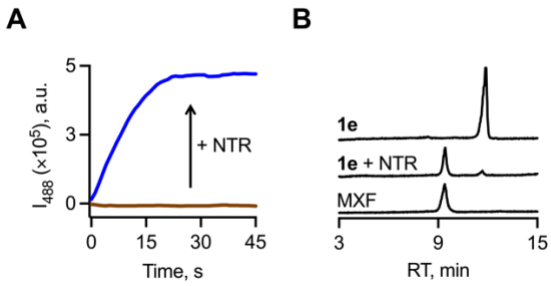

Figure 3. NTR mediated nitro-reduction of **1e** resulted in the release of MXF. (A) Time course of reaction of **1e** at 25 ºC without (-) or with (+) NTR (15 nM) and NADH (100 μM) in PB. (B) LC/MS analysis showing the representative total ion chromatograms (TICs) corresponding to the generation of MXF ([M+H]$^+$: expected = m/z 402.1824; observed = m/z 402.1826; eluted at 11.8 min) upon reacting **1e** (expected, [M+H]$^+$: expected = m/z 544.1661; observed = m/z 544.1664; eluted at 9.4 min) with NTR (15 nM) and NADH (100 μM) in PB (pH 7.4, 10 mM).

The derivative **1e** displayed no significant enhancement in fluorescence attributable to the formation of MXF in the presence of biologically relevant analytes such as thiols (Cys, GSH), reductants (Vit-C), amino acids (His), oxidizing agents (H_2O_2), esterase enzyme (Es), NADH or NTR alone supporting the selectivity of cleavage of **1e** under bioreductive conditions (Figure S12). Due to the poor expression of NTR under normal oxygen saturation, NTR-activated prodrugs have been used in delivering drugs to hypoxic cancer cells.[37-40] We tested if **1e** was cleaved in MEF (mouse embryonic fibroblast cells) under normoxic conditions and found that nearly all **1e** remained intact in 2 h and about 16% of MXF was produced in 4 h (Figure S13). On the contrary, when **1e** was exposed to lysates derived from NTR-expressing *E. coli,* a quantitative yield of MXF was recorded (Figure S14) and diminished MXF yields with heat-inactivated lysate and NTR-inhibitor (dicoumarol).[41] Together these data demonstrated that **1e** was rapidly and selectively activated under bioreductive conditions to give MXF in an excellent yield.

Computational studies. To further understand the mechanism of action, we performed docking studies followed by molecular dynamic simulations. We conceived three possible mechanistic scenarios as illustrated in Figure 4A *viz.*(1) proton transfer (PT) followed by a formal hydride transfer (2) a formal hydride transfer followed by a proton transfer and (3) two consecutive electron transfer (ET)−proton transfer sequences for the reduction of the nitro groups by NTR, the latter is consistent with the literature precedence observed for CB1954.[42] The prodrugs (**1a-1e**, **2a**, **2b**) were docked into the homodimer of an FMN-dependent NTR enzyme from *Escherichia coli* (PDB: 1DS7) (SwissDock)[43] (Figure S15). In addition, compounds were docked into the FMN-dependent NTR from *Mycobacterium smegmatis* (PDB: 2WZV) that shares a 35% sequence similarity with *E. coli* NTR[44] (Figure S16). Models with the best docking score were then simulated for further analysis. Molecular dynamic (MD) simulations were performed utilizing the Amber program[45] with the general amber force field

(GAFF). An 8 nm water box solvated using TIP3P water models and minimized without restraints was used for production runs. Simulated annealing was carried out with 2ns equilibration and a 1fs time step to take the system to 300K. SHAKE algorithm constraints were applied to the waters and LINCS hydrogen bond constraints were applied to the entire system. The equilibrated structures were then subjected to 5ns production runs using a Nosé-Hoover thermostat under NVT conditions with a 2fs time step. This process was performed on three independently docked structures for each prodrug-enzyme complex obtained from Swissdock.[43] An average structure from the last 50fs of each production run was utilized to determine the average distance between the FMN cofactor and the nitrogen atom of the nitro moiety. The distances between the cofactor and the nitro group of the prodrugs ranged from 6.4 – 8.2 Å with an average of 7.4 Å (Figure 4B). Based on the distances obtained from the MD simulations described above, a direct hydride transfer from FMN is unlikely. Furthermore, the abundance of water in the active site supports an electron transfer followed by protonation via water as a possible mechanistic scenario. Furthermore, the computed driving force for electron transfer from FMN to each of the prodrugs can be used to indirectly infer the electron transfer barriers. This was done to circumvent complex computations needed to identify the outer sphere reorganization energy inside the enzyme active site. As demonstrated above, the computed driving forces summarized in Table 3 exhibit a positive correlation with the catalytic efficiency (k_{cat} /K_m) measured for *E. coli* NTR suggesting a rate-limiting influence of electron transfer, further validating our mechanistic hypothesis. These results are in agreement with the observations made by Wilke and coworkers[42] in similar NTR activated prodrugs.

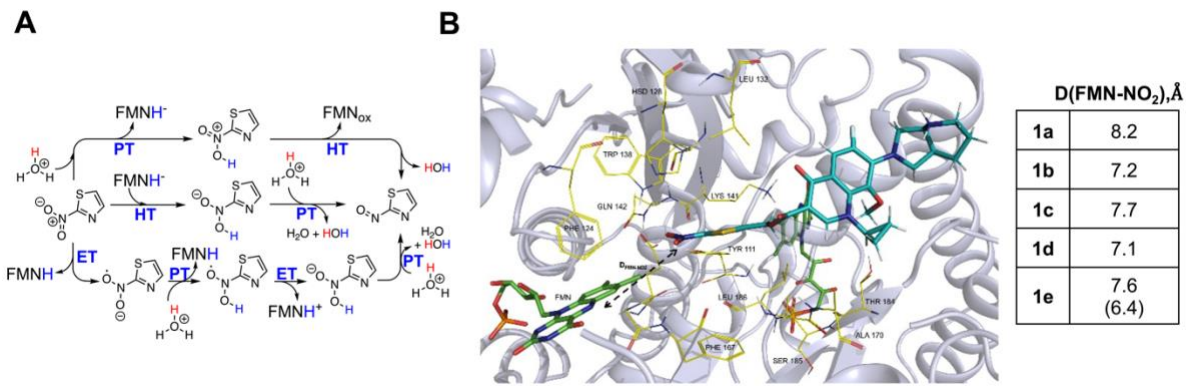

Figure 4. (A) Possible mechanistic scenarios for the reduction of 2-nitrothiazole functionality by *E. coli* NTR: (a) Hydride transfer (HT) from reduced flavin and subsequent proton transfer (PT) from solvent or (b) Electron transfer (ET) from reduced flavin accompanied with PT. (B) MD simulation model of **1e** in *E. coli* NTR (PDB: 1DS7). The key residues in the active site are shown in yellow. The distance [D(FMN-NO_2)] between the FMN residue and **1e** was 7.6 Å in *E. coli* NTR [PDB: 1DS7] and 6.4 Å in *Msm* NTR [PDB: 1DS7] respectively.

Comparison of 1e and MXF in replicating bacteria. The prodrug was next compared with MXF in laboratory strain *Mtb* H37Rv, and patient-derived multi-drug resistant (MDR), and extensively drug resistant (XDR) strains using an Alamar blue (AB) assay. The minimum inhibitory concentration (MIC) of prodrug **1e** and MXF was identical in all the aforementioned strains (Figure 5A). Next, MXF and the prodrug were compared in a phorbol myristate acetate (PMA)-differentiated THP-1 macrophages infection model, and again, the bactericidal activity of **1e** and MXF were similar suggesting that the prodrug was effective in reducing mycobacterial burden inside macrophages (Figure 5B).

We have recently reported that MXF induces reactive oxygen species (ROS) and suppresses respiration in *Mtb*.[15] Therefore, we compared redox and respiratory changes in *Mtb* upon exposure to **1e** and MFX. We used a *Mtb* strain that expresses the redox biosensor Mrx1-roGFP2 from a plasmid (strain Mtb-roGFP2). Mrx1-roGFP2 is a ratiometric fluorescent biosensor that reports the redox potential of the mycothiol redox couple (reduced mycothiol[MSH]/oxidized mycothiol [MSSM]) in the cytoplasm of *Mtb*.[46] An increase in

biosensor ratio indicates oxidative stress, whereas reductive stress decreases the biosensor ratio.[46]

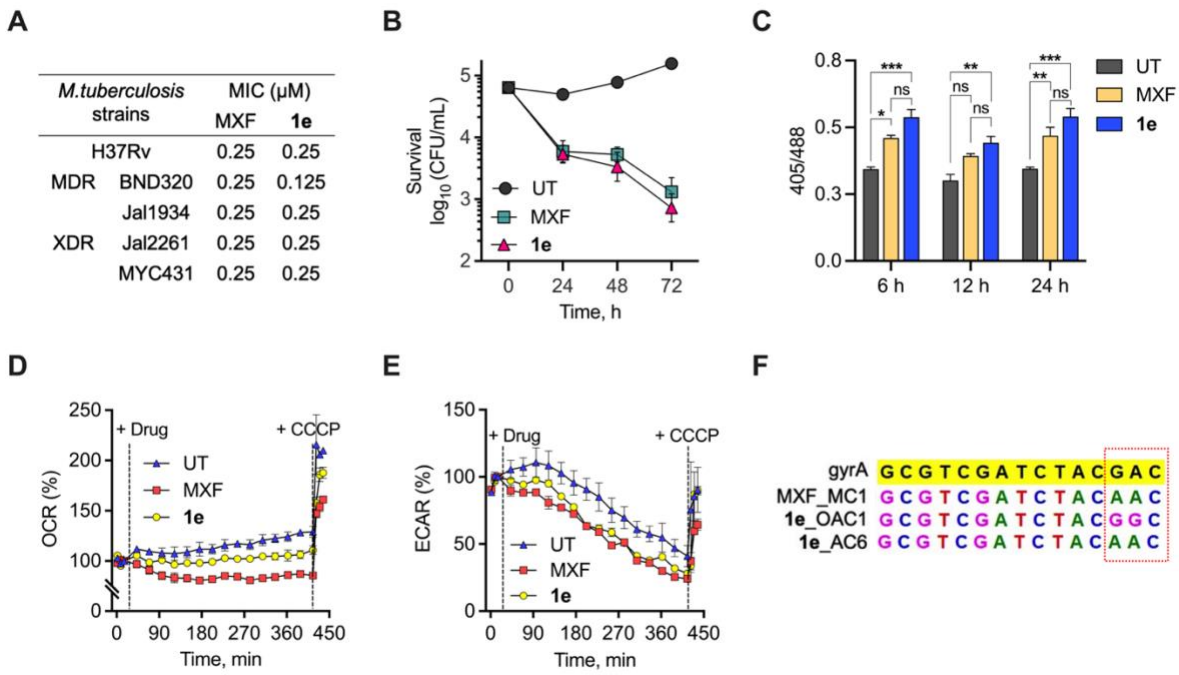

Figure 5. Bactericidal activity of **1e** against replicating *Mtb*. (A) Antimycobacterial activity of MXF and **1e** against drug-susceptible and patient-derived resistant strains of *Mtb*. (B) Bacterial survival kinetics after treatment of THP-1 macrophages infected with *Mtb* H37Rv at 5x MIC of **1e** and MXF. Results are expressed as mean ± SD from three independent experiments done in triplicate. (C) Ratiometric response of the biosensor following exposure of *Mtb*-roGFP2 to 10x MICs of MXF and **1e** at different intervals (6 h, 12 h and 24 h). Statistical significance was established relative to untreated bacteria control (UT) and MXF using Two-way ANOVA (* $p < 0.05$, ** $p \leq 0.01$, and *** $p \leq 0.001$). Determination of (D) OCR (pmol/min) indicated oxygen consumption rate and (E) ECAR (mpH/min) indicated H^+ production or extracellular acidification due to glycolytic and TCA flux by Seahorse XFp Analyzer. Exponentially growing *Mtb* cultures were either left untreated (UT) or treated with 10x MIC of MXF or **1e** for the indicated times; black dotted lines indicate when drug (MXF or **1e**, 10x MIC) or CCCP (10 μM) were added. The data was represented as percentage of baseline value. (F) Sequences of PCR amplified quinolone resistance determinant region (QRDR) using genomic DNA in gyrA of WT and resistant isolates from MXF (MC1) and **1e** (OAC1 and AC6) mutant prevention concentration (MPC) plate. The dotted box highlights the mutation from GAC (aspartic acid) to AAC (asparagine) in resistant colonies of MXF (MC1) and **1e** (OAC1) and to GGC (glycine) in resistant colony of **1e** (AC6).

Exposure to MXF or **1e** (2.5 μM; 10x MIC) induces comparable increase in the biosensor ratio over-time, indicating elevated oxidative stress (Figure 5C). For bioenergetics, we measured changes in the extracellular acidification rate (ECAR) and oxygen consumption rate (OCR) for MXF- or **1e**-treated *Mtb* as readouts for carbon metabolism (glycolysis and tricarboxylic acid [TCA] cycle) and for oxidative phosphorylation (OXPHOS), respectively, using a Seahorse XFp analyzer.[47,48] As expected for a normally growing *Mtb*, OCR showed a gradual increase over the duration of the experiment (400 min); OCR increased further upon uncoupling by carbonyl cyanide *m*-chlorophenylhydrazone (CCCP; addition of CCCP stimulates respiration to the maximal level) (Figure 5D). In contrast, addition of MXF or **1e** (2.5 μM; 10x MIC) inhibited the time-dependent increase in basal OCR.[15] Furthermore, the level of OCR upon uncoupling by CCCP was significantly lower in MXF or **1e**-treated *Mtb* than drug-free *Mtb*. A similar decrease in ECAR was observed upon treatment with MXF or **1e** (Figure 5E). Both MXF and **1e** suppressed OCR and ECAR to a similar degree. We earlier reported that *Mtb* maintains 100% survival in response to 10x MIC for ~ 10 h, confirming that diminished bioenergetics of *Mtb* by MXF or **1e** is not due to dead cells.[15] Lastly, we generated laboratory evolved mutants of *Mtb* in response to MXF and **1e** (Table S2) and confirmed that in both the cases mutations were mapped to the quinolone resistance determinant region (QRDR) of DNA gyrase A (gyrA)[49] (Figure 5F and S17).

In addition to the treatment of TB infections, MXF is widely used as a broad-spectrum antibiotic. The potency of **1e** against ESKAPE pathogens and NTMs was next evaluated using standard assays. Prodrug **1e** had nearly identical inhibitory profile as MXF in these pathogens as well as clinically derived drug-resistant pathogens (Figure S18A and S18B; Table S3, S4 and S5). We also found a similar reduction in bacterial burden in a neutropenic murine *E. coli* ATCC 25922 infected thigh model at comparable doses (Figure S19). Additionally, when **1e** was evaluated in fluoroquinolone-resistant *E. coli* mutants, we found a significantly higher

MIC value (MIC = 80 μM), which was comparable to MXF (MIC >100 μM) (Table S6). Hence, it appears that in both *Mtb* as well as *E. coli*, the prodrug **1e** and MXF have similar efficacy as well as mechanism of action.

Comparison of 1e and MXF in non-replicating *Mycobacterium tuberculosis*. The prodrug was next compared with MXF in non-replicating *Mtb*. A hypoxia resazurin reduction assay (HyRRA) was used to study growth inhibition in non-replicating *Mtb*. Isoniazid (INH) and Metronidazole (MZ) were used as controls. Under these conditions, consistent with literature reports, INH showed no significant growth inhibition while MZ inhibited growth at 10 mM concentrations. MXF had some effect on growth but the compound **1e** was found to have a significantly higher potency when compared with MXF (Figure 6A). Colonies generated from the aforementioned assay were plated and growth was measured and **1e** was significantly better than both MZ and MXF (Figure 6B).

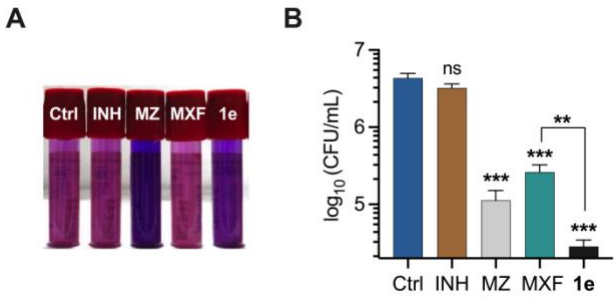

Figure 6. Bactericidal activity of **1e** against non-replicating *Mtb*. (A) Mycobactericidal effect of MXF and **1e** at indicated concentration (10x MIC, 2.5μM) on hypoxia-adapted *Mtb* bacilli based on visual hypoxia resazurin reduction assay (HyRRA). Isoniazid (INH, 10 μM) and Metronidazole (MZ, 10 mM) served as a negative and positive control respectively. The pink colour in the tube indicates cell viability under hypoxia while blue colour indicates no growth. (B) Survival of *Mtb* under hypoxia was measured as $\log_{10}$ of colony-forming units (CFU) after treatment with 10x MIC (2.5 μM) of MFX and **1e** for 5 days. Results are expressed as mean ± SD from three independent experiments performed in triplicate. Statistical significance was established relative to untreated bacteria control (Ctrl) using unpaired *t*-test with Welch's correction student's (ns indicate not significant, ** $p \leq 0.01$, and *** $p \leq 0.001$).

Intracellular accumulation of MXF and 1e. Mechanistic studies with replicating *Mtb* demonstrate that the action of **1e** is quite similar to MXF. In order to understand the intracellular accumulation of the drug when treated with MXF alone or prodrug **1e**, an LC/MS assay based on reported methods was developed (Figure 7A and S20).[14,50] Briefly, exponentially growing *Mtb* were incubated at 37 °C in PBS (1x, pH 7.4) with either MXF or **1e** at a final concentration of 5 μM. After incubation with the test compound for 30 min, replicating bacilli were pelleted by centrifugation through silicone oil mix and then lysed through bead beating. The compounds were extracted from the resultant lysate using PBS-MeOH and filtered through a 3 kDa Amicon® centrifugal filter. The intracellular concentrations were determined using a standard calibration curve (Figure S21 and S22), converted into accumulation values, then normalized with the bacterial count and were finally represented as MXF accumulation (nmol/10^8 CFUs). We find that in replicating *Mtb*, the accumulation of MXF in cells treated with **1e** was nearly identical to those treated with free MXF (Figure 7B). The intact prodrug **1e** could not be detected under these conditions. This result is consistent with our observation that **1e** was rapidly cleaved under bioreductive conditions (half-life < 1 min) to produce MXF in a nearly quantitative yield (Figure 3A and S10). Hence, our data suggests that **1e** and MXF have similar permeability and accumulation profiles in replicating *Mtb*.

Next, in non-replicating *Mtb*, a similar workflow was used to determine intracellular drug accumulation and whether this contributed to enhanced efficacy of **1e** over MXF. Under these conditions, we find a significant reduction in the amount of MXF in cells that were treated with the free drug. This observation is consistent with previous reports which show the free MXF was poorly accumulated in non-replicating *Mtb*. Under similar conditions when **1e** was used, we find a substantially higher intracellular accumulation of MXF (Figure 7C). Again, the intact prodrug **1e** could not be detected under these conditions.

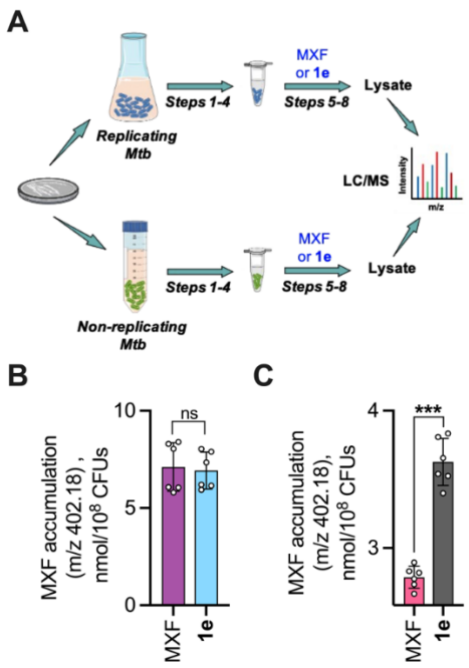

Figure 7. (A) Workflow for Accumulation assay. (B-C) LC-MS analysis of intracellular concentrations of MXF (m/z 402.18) in (B) exponentially growing and (C) hypoxic cultures of *Mtb*following incubation for 30 min with a fixed concentration of MXF and **1e** of 5 μM. The drug content is expressed as the amount of drug (nmol) per CFU. Statistical significance was established relative to MXF treated sample using unpaired *t*-test (ns indicate not significant and *** $p \leq 0.001$).

DISCUSSION

Mtb possesses a remarkable ability to evade host immune pressures and enter a quiescent state where most frontline antibiotics are ineffective.[5,51] The prevalence of non-replicating mycobacterial persisters are a major impediment to effective TB treatment. New regimens incorporating MXF and Rifapentine are promising but the lack of activity of MXF against non-replicating *Mtb* is yet a major concern and needs new interventional strategies.[13] The equilibrium between non-replicating and replicating bacilli serves as a defining characteristic between latent and active infection.[51,52] A recent study suggested that *Mtb* exists in a replicating state during the early latency and later transitions into a non-replicating state during prolonged latency.[53] The occurrences of latent tuberculosis, where the patient does not present symptoms

of TB is also attributed to non-replicating *Mtb* contributing to phenotypic AMR.[54] Hence, the need to eliminate both replicating and non-replicating *Mtb* is urgent. The adaptation into a drug-tolerant non-replicating persistent state is often associated with metabolic downshift and increased thickening of lipid-rich cell wall.[10,11,19] Metabolomic and lipidomic analysis demonstrated that non-replicating bacteria accumulate mycolate wax esters and long-chain triacylglycerol esters along with an increase in the ratio of lipoarabinomannan to lipomannan.[55,56] This distinct phenotype contributes to reduced penetration and intracellular accumulation of many antibiotics.[12] Our drug of choice was MXF, whose target gyrase is expressed in non-replicating *Mtb*.[17,18] Mass spectrometric studies revealed that the intracellular accumulation of MXF is diminished to a significant extent in nutrient starved non-replicating *Mtb*, which probably contributes to the marked reduction in bactericidal efficacy of MXF by more than 100-fold.[14] MXF was also found to be less effective against hypoxic non-replicating *Mtb.*[15] In this study, a prodrug approach that increased lipophilicity was exploited to enhance the permeation resulting in increased drug accumulation; the activation mechanism of the prodrug to generate MXF appears selective to bacteria. Here, we provide evidence that enhancing the amount of MXF using a prodrug within non-replicating *Mtb* has a tremendous impact on eliminating persisters. Non-replicating *Mtb* that reside in the hypoxic regions of granulomas strongly induce DevR regulon-controlled genes encoding several nitroreductases (NTRs) by several fold.[23,24,57] These NTRs probably contribute to combat nitrosative and oxidative stress encountered inside host macrophage to survive and establish infection.[58,59] Prodrug activation is achieved by nitroreductases that are expressed in non-replicating as well as in replicating *Mtb*, albeit at somewhat lower levels in the latter. Despite the nitro group being somewhat less favored in traditional medicinal chemistry, many clinically used TB drugs (Pretomanid,[60,61] Delamanid,[62,63] TB-354,[64] nitrofuranylcalonolides, and TP-053[65]) contain an essential nitro functional group. To identify a suitable prodrug, preliminary investigation was

conducted with commercially available *E. coli* NTR. The prodrug was rapidly activated under bioreductive conditions to provide MXF in quantitative yield. Detailed computational analysis was ascertained to determine the driving force for electron transfer from FMN to the nitro group, which supported the likelihood of electron transfer in prodrug activation. Notably, this prodrug was equipotent to MXF in its inhibitory activity in both cellular models and animal models. The newly developed prodrug demonstrated superior inhibitory activity against non-replicating *Mtb* when compared with MXF likely due to enhanced accumulation of drug. Our study demonstrates that enhancing permeability and accumulation of a clinical drug can have positive outcomes in inhibiting bacterial growth. The drug concentration within cells leading to adequate drug-target engagement that is necessary to induce lethality will vary from drug to drug. But since drug accumulation in non-replicating *Mtb* is uniformly low for all TB drugs, strategies that enhance bactericidal drug accumulation are expected to address a major clinical problem.[66]

CONCLUSION

We provide evidence for a prodrug approach against phenotypic AMR in *Mtb* by focusing on improving cell-permeability and drug accumulation, while optimizing for rapid, selective and efficient conversion within bacteria. This innovative strategy can, in principle, be extended to other clinical TB drugs and will complement approaches that either target and kill non-replicating bacilli or resuscitate/resensitize them to a drug-susceptible state. Although the development of new molecules with novel targets is important, the discovery and subsequent introduction of new antibiotics into the global market has been a slow, expensive and cumbersome process. Hence, the methodology developed herein provides a sound framework for future prodrug design that can optimize for enhancing accumulation of the active drug to eliminate persisters and potentially improve treatment outcomes.

Corresponding Authors

* jhirschi@binghamton.edu; asingh@iisc.ac.in; harinath@iiserpune.ac.in

ACKNOWLEDGMENT

Financial support for this project was from IISER Pune, Department of Science and Technology (DST) Fund for Improvement of S&T Infrastructure (grant number SR/FST/LSII-043/2016) to the IISER Pune Biology Department for setting up the Biological Mass Spectrometry Facility and Ignite Life Sciences for LC/MS studies. Research fellowship for TAK and GK (DST-INSPIRE), AA thanks UGC. The authors thank Mr. Arnab Chakraborty (Dr. Siddhesh S. Kamat Lab, IISER Pune) and Mrs. Sunita (LC/MS facility incharge, IISc, Bangalore).

ABBREVIATIONS

AB, alamar blue; AMR, Antimicrobial resistance; CCCP, carbonyl cyanide *m*-chlorophenylhydrazone, CFU, colony forming unit; ET, electron transfer; *E. coli*, *Escherichia coli*; ECAR, extracellular acidification rate; FMN, flavin mononucleotide; HyRRA, hypoxia resazurin reduction assay; INH, isoniazid; *Mtb*, Mycobacterium tuberculosis; MXF, Moxifloxacin; MR, Molar refractivity; *Msm*, *Mycobacterium smegmatis*; MDR, multi-drug resistant; MD, molecular dynamics; MIC, minimum inhibitory concentration; MZ, metronidazole; NTR, Nitroreductase; NTM, non-tuberculosis mycobacteria; OCR, oxygen consumpton rate; OXPHOS, oxidative phosphorylation; PT, proton transfer; QRDR, quinolone resistance determinant region; ROS, reactive oxygen species; TPSA, topological polar surface area; TIC, total ion chromatograms; TCA, tricarboxylic acid cycle; TB, Tuberculosis; XDR, extensively drug-resistant.

REFERENCES

(1) World Health Organization, *Global Tuberculosis Report 2021;* WHO: Geneva, **2021**, 1-27.

(2) Paulson, T. Epidemiology: A Mortal Foe. *Nature* **2013**, *502* (7470), S2–S3. https://doi.org/10.1038/502S2a.

(3) Zumla, A.; Nahid, P.; Cole, S. T. Advances in the Development of New Tuberculosis Drugs and Treatment Regimens. *Nat. Rev. Drug Discov*. **2013**, *12*, 388–404. https://doi.org/10.1038/nrd4001.

(4) Horsburgh, C. R.; Barry, C. E.; Lange, C. Treatment of Tuberculosis. *New Eng. J. Med.* **2015**, *373* (22), 2149–2160. https://doi.org/10.1056/NEJMra1413919.

(5) Manina, G.; Dhar, N.; McKinney, J. D. Stress and Host Immunity Amplify Mycobacterium Tuberculosis Phenotypic Heterogeneity and Induce Nongrowing Metabolically Active Forms. *Cell Host Microbe* **2015**, *17* (1), 32–46. https://doi.org/10.1016/j.chom.2014.11.016.

(6) Ahmed, M.; Mackenzie, J.; Tezera, L.; Krause, R.; Truebody, B.; Garay-Baquero, D.; Vallejo, A.; Govender, K.; Adamson, J.; Fisher, H.; Essex, J. W.; Mansour, S.; Elkington, P.; Steyn, A. J. C.; Leslie, A. Mycobacterium Tuberculosis Senses Host Interferon-γ via the Membrane Protein MmpL10. *Commun. Biol.* **2022**, *5* (1), 1317. https://doi.org/10.1038/s42003-022-04265-0.

(7) Cohen, N. R.; Lobritz, M. A.; Collins, J. J. Microbial Persistence and the Road to Drug Resistance. *Cell Host Microbe* **2013**, 632–642. https://doi.org/10.1016/j.chom.2013.05.009.

(8) Sebastian, J.; Swaminath, S.; Nair, R. R.; Jakkala, K.; Pradhan, A.; Ajitkumar, P. De Novo Emergence of Genetically Resistant Mutants of Mycobacterium Tuberculosis from the Persistence Phase Cells Formed against Antituberculosis Drugs in Vitro. *Antimicrob. Agents Chemother*. **2017**, *61* (2). https://doi.org/10.1128/AAC.01343-16.

(9) Zhang, Y. Persisters, Persistent Infections and the Yin-Yang Model. *Emerg. Microbes Infect*. **2014**. *3* (1), e3. https://doi.org/10.1038/emi.2014.3.

(10) Vilchèze, C.; Yan, B.; Casey, R.; Hingley-Wilson, S.; Ettwiller, L.; Jacobs, W. R. Commonalities of Mycobacterium Tuberculosis Transcriptomes in Response to Defined Persisting Macrophage Stresses. *Front. Immunol.* **2022**, *13* (909904), 1-18. https://doi.org/10.3389/fimmu.2022.909904.

(11) Stokas, H.; Rhodes, H. L.; Purdy, G. E. Modulation of the M. Tuberculosis Cell Envelope between Replicating and Non-Replicating Persistent Bacteria. *Tuberculosis (Edinb).* **2020**, *125*, 102007. https://doi.org/10.1016/j.tube.2020.102007.

(12) Cunningham, A. F.; Spreadbury, C. L. Mycobacterial Stationary Phase Induced by Low Oxygen Tension: Cell Wall Thickening and Localization of the 16-Kilodalton-Crystallin Homology. *J. Bacteriol.* **1998**, *180* (4), 801-8. https://journals.asm.org/journal/jb.

(13) Dorman, S. E.; Nahid, P.; Kurbatova, E. V.; Phillips, P. P. J.; Bryant, K.; Dooley, K. E.; Engle, M.; Goldberg, S. V.; Phan, H. T. T.; Hakim, J.; Johnson, J. L.; Lourens, M.; Martinson, N. A.; Muzanyi, G.; Narunsky, K.; Nerette, S.; Nguyen, N. V.; Pham, T. H.; Pierre, S.; Purfield, A. E.; Samaneka, W.; Savic, R. M.; Sanne, I.; Scott, N. A.; Shenje, J.; Sizemore, E.; Vernon, A.; Waja, Z.; Weiner, M.; Swindells, S.; Chaisson, R. E. Four-Month Rifapentine Regimens with or without Moxifloxacin for Tuberculosis. *New Eng. J. Med.* **2021**, *384* (18), 1705–1718. https://doi.org/10.1056/nejmoa2033400.

(14) Sarathy, J.; Dartois, V.; Dick, T.; Gengenbacher, M. Reduced Drug Uptake in Phenotypically Resistant Nutrient-Starved Nonreplicating Mycobacterium Tuberculosis. *Antimicrob. Agents Chemother*. **2013**, *57* (4), 1648–1653. https://doi.org/10.1128/AAC.02202-12.

(15) Somnath, S.; Samsher, S.; Ashutosh, T.; Chandrani, T.; Anand, K. T.; Mayashree, D.; Vikas, Y.; Sakshi, K.; S, R. R.; Nagasuma, C.; Harinath, C.; Karl, D.; Amit, S. Moxifloxacin-Mediated Killing of Mycobacterium Tuberculosis Involves Respiratory Downshift, Reductive Stress, and Accumulation of Reactive Oxygen Species. *Antimicrob. Agents Chemother*. **2022**, *66* (9), e00592-22. https://doi.org/10.1128/aac.00592-22.

(16) Mustaev, A.; Malik, M.; Zhao, X.; Kurepina, N.; Luan, G.; Oppegard, L. M.; Hiasa, H.; Marks, K. R.; Kerns, R. J.; Berger, J. M.; Drlica, K. Fluoroquinolone-Gyrase-DNA Complexes. *J. Biol. Chem.* **2014**, *289* (18), 12300–12312. https://doi.org/10.1074/jbc.M113.529164.

(17) Sala, C.; Dhar, N.; Hartkoorn, R. C.; Zhang, M.; Ha, Y. H.; Schneider, P.; Cole, S. T. Simple Model for Testing Drugs against Nonreplicating *Mycobacterium Tuberculosis*. *Antimicrob. Agents Chemother*. **2010**, *54* (10), 4150–4158. https://doi.org/10.1128/AAC.00821-10.

(18) Chopra, S.; Matsuyama, K.; Tran, T.; Malerich, J. P.; Wan, B.; Franzblau, S. G.; Lun, S.; Guo, H.; Maiga, M. C.; Bishai, W. R.; Madrid, P. B. Evaluation of Gyrase B as a Drug Target in Mycobacterium Tuberculosis. *J. Antimicrob. Chemother.* **2012**, *67* (2), 415–421. https://doi.org/10.1093/jac/dkr449.

(19) Jakkala, K.; Ajitkumar, P. Hypoxic Non-Replicating Persistent Mycobacterium Tuberculosis Develops Thickened Outer Layer That Helps in Restricting Rifampicin Entry. *Front. Microbiol.* **2019**, *10*, 2339. https://doi.org/10.3389/fmicb.2019.02339.

(20) Langlois, M.H.; Montagut, M.; Dubost, J.P.; Grellet, J.; Saux, M.C. Protonation Equilibrium and Lipophilicity of Moxifloxacin. *J. Pharm. Biomed. Anal.***2005**, *37* (2), 389–393. https://doi.org/10.1016/j.jpba.2004.10.022.

(21) Hudock, T. A.; Foreman, T. W.; Bandyopadhyay, N.; Gautam, U. S.; Veatch, A. V.; LoBato, D. N.; Gentry, K. M.; Golden, N. A.; Cavigli, A.; Mueller, M.; Hwang, S.-A.; Hunter, R. L.; Alvarez, X.; Lackner, A. A.; Bader, J. S.; Mehra, S.; Kaushal, D. Hypoxia Sensing and Persistence Genes Are Expressed during the Intragranulomatous Survival of *Mycobacterium Tuberculosis*. *Am. J. Respir. Cell Mol. Biol.***2017**, *56* (5), 637–647. https://doi.org/10.1165/rcmb.2016-0239OC.

(22) Belton, M.; Brilha, S.; Manavaki, R.; Mauri, F.; Nijran, K.; Hong, Y. T.; Patel, N. H.; Dembek, M.; Tezera, L.; Green, J.; Moores, R.; Aigbirhio, F.; Al-Nahhas, A.; Fryer, T. D.; Elkington, P. T.; Friedland, J. S. Hypoxia and Tissue Destruction in Pulmonary TB. *Thorax* **2016**, *71* (12), 1145–1153. https://doi.org/10.1136/thoraxjnl-2015-207402.

(23) Chauhan, S.; Sharma, D.; Singh, A.; Surolia, A.; Tyagi, J. S. Comprehensive Insights into Mycobacterium Tuberculosis DevR (DosR) Regulon Activation Switch. *Nucleic Acids Res.***2011**, *39* (17), 7400–7414. https://doi.org/10.1093/nar/gkr375.

(24) Sherman, D. R.; Voskuil, M.; Schnappinger, D.; Liao, R.; Harrell, M. I.; Schoolnik, G. K. Regulation of the Mycobacterium Tuberculosis Hypoxic Response Gene Encoding α-Crystallin. *Proc. Natl. Acad. Sci. U. S. A.* **2001**, *98* (13), 7534-9. https://doi.org/10.1073/pnas.121172498.

(25) Tanaka, K. S. E.; Houghton, T. J.; Kang, T.; Dietrich, E.; Delorme, D.; Ferreira, S. S.; Caron, L.; Viens, F.; Arhin, F. F.; Sarmiento, I.; Lehoux, D.; Fadhil, I.; Laquerre, K.; Liu, J.; Ostiguy, V.; Poirier, H.; Moeck, G.; Parr, T. R.; Rafai Far, A. Bisphosphonated Fluoroquinolone Esters as Osteotropic Prodrugs for the Prevention of Osteomyelitis. *Bioorg. Med. Chem.* **2008**, *16* (20), 9217–9229. https://doi.org/10.1016/J.BMC.2008.09.010.

(26) Machado, D.; Girardini, M.; Viveiros, M.; Pieroni, M. Challenging the Drug-Likeness Dogma for New Drug Discovery in Tuberculosis. *Front. Microbiol.* **2018**, *9* (1367), 1-23. https://doi.org/10.3389/fmicb.2018.01367.

(27) Daina, A.; Michielin, O.; Zoete, V. SwissADME: A Free Web Tool to Evaluate Pharmacokinetics, Drug-Likeness and Medicinal Chemistry Friendliness of Small Molecules. *Sci. Rep.* **2017**, *7* (42717), 1-13.

(28) Chai, J.-D.; Head-Gordon, M. Long-Range Corrected Hybrid Density Functionals with Damped Atom–Atom Dispersion Corrections. *Phys. Chem. Chem. Phys.* **2008**, *10* (44), 6615. https://doi.org/10.1039/b810189b.

(29) Becke, A. D. Density-functional Thermochemistry. III. The Role of Exact Exchange. *J. Chem. Phys.***1993**, *98* (7), 5648–5652. https://doi.org/10.1063/1.464913.

(30) Hehre, W. J.; Stewart, R. F.; Pople, J. A. Self-Consistent Molecular-Orbital Methods. I. Use of Gaussian Expansions of Slater-Type Atomic Orbitals. *J. Chem. Phys.* **1969**, *51* (6), 2657–2664. https://doi.org/10.1063/1.1672392.

(31) Viola, G.; Facciolo, L.; Canton, M.; Vedaldi, D.; Dall'Acqua, F.; Aloisi, G. G.; Amelia, M.; Barbafina, A.; Elisei, F.; Latterini, L. Photophysical and Phototoxic Properties of the Antibacterial Fluoroquinolones Levofloxacin and Moxifloxacin. *Chem. Biodivers.* **2004**, *1* (5), 782–801. https://doi.org/10.1002/cbdv.200490061.

(32) Wang, J.; Liu, J.; Yang, Z. Recent Advances in Peptide-Based Nanomaterials for Targeting Hypoxia. *Nanoscale Adv.* **2021**, *3*, 6027–6039. https://doi.org/10.1039/d1na00637a.

(33) Pardeshi, K. A.; Kumar, T. A.; Ravikumar, G.; Shukla, M.; Kaul, G.; Chopra, S.; Chakrapani, H. Targeted Antibacterial Activity Guided by Bacteria-Specific Nitroreductase Catalytic Activation to Produce Ciprofloxacin. *Bioconjug. Chem.***2019**, *30* (3), 751–759. https://doi.org/10.1021/acs.bioconjchem.8b00887.

(34) Wang, S.; Wu, X.; Zhang, Y.; Zhang, D.; Xie, B.; Pan, Z.; Ouyang, K.; Peng, T. Discovery of a Highly Efficient Nitroaryl Group for Detection of Nitroreductase and

Imaging of Hypoxic Tumor Cells. *Org. Biomol. Chem.* **2021**, *19* (15), 3469–3478. https://doi.org/10.1039/d1ob00356a.

(35) Gruber, T. D.; Krishnamurthy, C.; Grimm, J. B.; Tadross, M. R.; Wysocki, L. M.; Gartner, Z. J.; Lavis, L. D. Cell-Specific Chemical Delivery Using a Selective Nitroreductase-Nitroaryl Pair. *ACS Chem. Biol.* **2018**, *13* (10), 2888–2896. https://doi.org/10.1021/acschembio.8b00524.

(36) Herrlinger, E.-M.; Hau, M.; Melanie Redhaber, D.; Greve, G.; Willmann, D.; Steimle, S.; Müller, M.; Lübbert, M.; Cornelius Miething, C.; Schüle, R.; Jung, M. Nitroreductase-Mediated Release of Inhibitors of Lysine-Specific Demethylase 1 (LSD1) from Prodrugs in Transfected Acute Myeloid Leukaemia Cells.*ChemBioChem.* **2020**, *21* (16), 2329-2347.https://doi.org/10.26434/chemrxiv.10012937.v1.

(37) Sun, Z.; Zhang, H.; Zhang, H.; Wu, J.; Gao, F.; Zhang, C.; Hu, X.; Liu, Q.; Wei, Y.; Wei, Y.; Zhuang, J.; Zhuang, J.; Huang, X. A Novel Model System for Understanding Anticancer Activity of Hypoxia-Activated Prodrugs. *Mol. Pharm.* **2020**, *17* (6), 2072–2082. https://doi.org/10.1021/acs.molpharmaceut.0c00232.

(38) O'Connor, L. J.; Cazares-Körner, C.; Saha, J.; Evans, C. N. G.; Stratford, M. R. L.; Hammond, E. M.; Conway, S. J. Design, Synthesis and Evaluation of Molecularly Targeted Hypoxia-Activated Prodrugs. *Nat. Protoc.* **2016**, *11* (4), 781–794. https://doi.org/10.1038/nprot.2016.034.

(39) Winn, B. A.; Shi, Z.; Carlson, G. J.; Wang, Y.; Nguyen, B. L.; Kelly, E. M.; Ross, R. D.; Hamel, E.; Chaplin, D. J.; Trawick, M. L.; Pinney, K. G. Bioreductively Activatable Prodrug Conjugates of Phenstatin Designed to Target Tumor Hypoxia. *Bioorg. Med. Chem. Lett.* **2017**, *27* (3), 636-641.

(40) Jin, C.; Zhang, Q.; Lu, W. Synthesis and Biological Evaluation of Hypoxia-Activated Prodrugs of SN-38. *Eur. J. Med. Chem.* **2017**, *132*, 135-141.

(41). Johansson, E.; Parkinson, G. N.; Denny, W. A.; Neidle, S. Studies on the Nitroreductase Prodrug-Activating System. Crystal Structures of Complexes with the Inhibitor Dicoumarol and Dinitrobenzamide Prodrugs and of the Enzyme Active Form. *J. Med. Chem.* **2003**, *46* (19), 4009–4020. https://doi.org/10.1021/jm030843b.

(42) Christofferson, A.; Wilkie, J. Mechanism of CB1954 Reduction by *Escherichia Coli* Nitroreductase. *Biochem. Soc. Trans.* **2009**, *37* (2), 413–418. https://doi.org/10.1042/BST0370413.

(43) Grosdidier, A.; Zoete, V.; Michielin, O. SwissDock, a Protein-Small Molecule Docking Web Service Based on EADock DSS. *Nucleic Acids Res.***2011**, *39*, W270–W277. https://doi.org/10.1093/nar/gkr366.

(44) Manina, G.; Bellinzoni, M.; Pasca, M. R.; Neres, J.; Milano, A.; De Jesus Lopes Ribeiro, A. L.; Buroni, S.; Škovierová, H.; Dianišková, P.; Mikušová, K.; Marák, J.; Makarov, V.; Giganti, D.; Haouz, A.; Lucarelli, A. P.; Degiacomi, G.; Piazza, A.; Chiarelli, L. R.; De Rossi, E.; Salina, E.; Cole, S. T.; Alzari, P. M.; Riccardi, G. Biological and Structural Characterization of the Mycobacterium Smegmatis Nitroreductase NfnB, and Its Role

in Benzothiazinone Resistance. *Mol. Microbiol.* **2010**, *77* (5), 1172–1185. https://doi.org/10.1111/j.1365-2958.2010.07277.x.

(45) Case, D. A.; Cheatham, T. E.; Darden, T.; Gohlke, H.; Luo, R.; Merz, K. M.; Onufriev, A.; Simmerling, C.; Wang, B.; Woods, R. J. The Amber Biomolecular Simulation Programs. *J. Comput. Chem.* **2005**, *26* (16), 1668–1688. https://doi.org/10.1002/jcc.20290.

(46) Bhaskar, A.; Chawla, M.; Mehta, M.; Parikh, P.; Chandra, P.; Bhave, D.; Kumar, D.; Carroll, K. S.; Singh, A. Reengineering Redox Sensitive GFP to Measure Mycothiol Redox Potential of Mycobacterium Tuberculosis during Infection. *PLoS Pathog.* **2014**, *10* (1), e1003902. https://doi.org/10.1371/journal.ppat.1003902.

(47) Lamprecht, D. A.; Finin, P. M.; Rahman, Md. A.; Cumming, B. M.; Russell, S. L.; Jonnala, S. R.; Adamson, J. H.; Steyn, A. J. C. Turning the Respiratory Flexibility of Mycobacterium Tuberculosis against Itself. *Nat. Commun.***2016**, *7* (1), 12393. https://doi.org/10.1038/ncomms12393.

(48) Mishra, R.; Kohli, S.; Malhotra, N.; Bandyopadhyay, P.; Mehta, M.; Munshi, M.; Adiga, V.; Ahuja, V. K.; Shandil, R. K.; Rajmani, R. S.; Seshasayee, A. S. N.; Singh, A. Targeting Redox Heterogeneity to Counteract Drug Tolerance in Replicating *Mycobacterium Tuberculosis*. *Sci. Transl. Med.* **2019**, *11* (518). https://doi.org/10.1126/scitranslmed.aaw6635.

(49) Sirgel, F. A.; Warren, R. M.; Streicher, E. M.; Victor, T. C.; van Helden, P. D.; Bottger, E. C. GyrA Mutations and Phenotypic Susceptibility Levels to Ofloxacin and Moxifloxacin in Clinical Isolates of Mycobacterium Tuberculosis. *J. Antimicrob. Chemother.* **2012**, *67* (5), 1088–1093. https://doi.org/10.1093/jac/dks033.

(50) Geddes, E. J.; Li, Z.; Hergenrother, P. J. An LC-MS/MS Assay and Complementary Web-Based Tool to Quantify and Predict Compound Accumulation in E. coli. *Nat. Protoc.* **2021**, *16* (10), 4833–4854. https://doi.org/10.1038/s41596-021-00598-y.

(51) Dhar, N.; Mckinney, J.; Manina, G. Phenotypic Heterogeneity in Mycobacterium Tuberculosis. *Microbiol. Spectr.* **2016**, *4* (6), 1-27. https://doi.org/10.1128/microbiolspec.TBTB2-0021.

(52) Esmail, H.; Barry, C. E.; Young, D. B.; Wilkinson, R. J. The Ongoing Challenge of Latent Tuberculosis. *Philos. Trans. R. Soc. Lond. B. Biol. Sci.* **2014**, *369* (1645), 20130437. https://doi.org/10.1098/rstb.2013.0437.

(53) Colangeli, R.; Gupta, A.; Vinhas, S. A.; Chippada Venkata, U. D.; Kim, S.; Grady, C.; Jones-López, E. C.; Soteropoulos, P.; Palaci, M.; Marques-Rodrigues, P.; Salgame, P.; Ellner, J. J.; Dietze, R.; Alland, D. Mycobacterium Tuberculosis Progresses through Two Phases of Latent Infection in Humans. *Nat. Commun.***2020**, *11* (1), 1-10. https://doi.org/10.1038/s41467-020-18699-9.

(54) Zhang, Y.; Yew, W. W.; Barer, M. R. Targeting Persisters for Tuberculosis Control. *Antimicrob. Agents Chemother*. **2012**, *56* (5), 2223-30. https://doi.org/10.1128/AAC.06288-11.

(55) Wright, C. C.; Hsu, F. F.; Arnett, E.; Dunaj, J. L.; Davidson, P. M.; Pacheco, S. A.; Harriff, M. J.; Lewinsohn, D. M.; Schlesinger, L. S.; Purdy, G. E. The Mycobacterium Tuberculosis MmpL11 Cell Wall Lipid Transporter Is Important for Biofilm Formation, Intracellular Growth, and Nonreplicating Persistence. *Infect. Immun.***2017**, *85* (8), e00131-17. https://doi.org/10.1128/IAI.

(56) Bacon, J.; Alderwick, L. J.; Allnutt, J. A.; Gabasova, E.; Watson, R.; Hatch, K. A.; Clark, S. O.; Jeeves, R. E.; Marriott, A.; Rayner, E.; Tolley, H.; Pearson, G.; Hall, G.; Besra, G. S.; Wernisch, L.; Williams, A.; Marsh, P. D. Non-Replicating Mycobacterium Tuberculosis Elicits a Reduced Infectivity Profile with Corresponding Modifications to the Cell Wall and Extracellular Matrix. *PLoS One***2014**, *9* (2). https://doi.org/10.1371/journal.pone.0087329.

(57) Dong, W.; Shi, J.; Chu, P.; Liu, R.; Wen, S.; Zhang, T.; Pang, Y.; Lu, J. Rv3131, a gene encoding nitroreductase, isessential for Metronidazole Activation in Mycobacterium Tuberculosis under Hypoxic Condition. *Res. Sq.***2020**, 1–15.

(58) Peddireddy, V.; Doddam, S. N.; Qureshi, I. A.; Yerra, P.; Ahmed, N. A Putative Nitroreductase from the DosR Regulon of Mycobacterium Tuberculosis Induces Pro-Inflammatory Cytokine Expression via TLR2 Signaling Pathway. *Sci. Rep.***2016**, *6*, 1–9. https://doi.org/10.1038/srep24535.

(59) Hu, Y.; Coates, A. R. M. Mycobacterium Tuberculosis Acg Gene Is Required for Growth and Virulence in Vivo. *PLoS One.***2011**, *6* (6), e20958. https://doi.org/10.1371/journal.pone.0020958.

(60) Singh, R.; Manjunatha, U.; Boshoff, H. I. M.; Young, H. H.; Niyomrattanakit, P.; Ledwidge, R.; Dowd, C. S.; Ill, Y. L.; Kim, P.; Zhang, L.; Kang, S.; Keller, T. H.; Jiricek, J.; Barry, C. E. PA-824 Kills Nonreplicating Mycobacterium Tuberculosis by Intracellular NO Release. . *Science.* **2008**, *322* (5906), 1392–1395. https://doi.org/10.1126/science.1164571.

(61) Conradie, F.; Bagdasaryan, T. R.; Borisov, S.; Howell, P.; Mikiashvili, L.; Ngubane, N.; Samoilova, A.; Skornykova, S.; Tudor, E.; Variava, E.; Yablonskiy, P.; Everitt, D.; Wills, G. H.; Sun, E.; Olugbosi, M.; Egizi, E.; Li, M.; Holsta, A.; Timm, J.; Bateson, A.; Crook, A. M.; Fabiane, S. M.; Hunt, R.; McHugh, T. D.; Tweed, C. D.; Foraida, S.; Mendel, C. M.; Spigelman, M. Bedaquiline–Pretomanid–Linezolid Regimens for Drug-Resistant Tuberculosis. *New Eng. J. Med.* **2022**, *387* (9), 810–823. https://doi.org/10.1056/NEJMoa2119430.

(62) Matsumoto, M.; Hashizume, H.; Tomishige, T.; Kawasaki, M.; Tsubouchi, H.; Sasaki, H.; Shimokawa, Y.; Komatsu, M. OPC-67683, a Nitro-Dihydro-Imidazooxazole Derivative with Promising Action against Tuberculosis in Vitro and in Mice. *PLoS Med.***2006**, *3* (11), 2131–2144. https://doi.org/10.1371/journal.pmed.0030466.

(63) Kim, C. T.; Kim, T.-O.; Shin, H.-J.; Ko, Y. C.; Hun Choe, Y.; Kim, H.-R.; Kwon, Y.-S. Bedaquiline and Delamanid for the Treatment of Multidrug-Resistant Tuberculosis: A

Multicentre Cohort Study in Korea. *Eur. Respir. J.* **2018**, *51* (3), 1702467. https://doi.org/10.1183/13993003.02467-2017.

(64) Upton, A. M.; Cho, S.; Yang, T. J.; Kim, A. Y.; Wang, Y.; Lu, Y.; Wang, B.; Xu, J.; Mdluli, K.; Ma, Z.; Franzblaub, S. G. In Vitro and in Vivo Activities of the Nitroimidazole TBA-354 against Mycobacterium Tuberculosis. *Antimicrob. Agents Chemother.***2015**, *59* (1), 136–144. https://doi.org/10.1128/AAC.03823-14.

(65) Albesa-Jové, D.; Chiarelli, L. R.; Makarov, V.; Pasca, M. R.; Urresti, S.; Mori, G.; Salina, E.; Vocat, A.; Comino, N.; Mohorko, E.; Ryabova, S.; Pfieiffer, B.; Lopes Ribeiro, A. L. D. J.; Rodrigo-Unzueta, A.; Tersa, M.; Zanoni, G.; Buroni, S.; Altmann, K. H.; Hartkoorn, R. C.; Glockshuber, R.; Cole, S. T.; Riccardi, G.; Guerin, M. E. Rv2466c Mediates the Activation of TP053 to Kill Replicating and Non-Replicating Mycobacterium Tuberculosis. *ACS Chem. Biol.***2014**, *9* (7), 1567–1575. https://doi.org/10.1021/cb500149m.

(66) Mabhula, A. N. Investigating permeation of anti-mycobacterial agents in *Mycobacterium tuberculosis* and *M. tuberculosis*-infected macrophages in vitro as a model for early stage tuberculosis drug discovery. Ph.D. dissertation, University of Cape Town, South Africa, 2020.